


Correlation between diffusion-weighted image-derived parameters and dynamic contrast-enhanced magnetic resonance imaging-derived parameters in the orofacial region

Acta Radiologica Open
13(3) 1–9
© The Author(s) 2024
Article reuse guidelines:
sagepub.com/journals-permissions
DOI: 10.1177/20584601241244777
journals.sagepub.com/home/arr


Toru Chikui¹ , Masahiro Ohga², Yukiko Kami¹ , Osamu Togao³, Shintaro Kawano⁴, Tamotsu Kiyoshima⁵ and Kazunori Yoshiura^{1,2}

Abstract

Background: Diffusion-weighted imaging (DWI) and dynamic contrast-enhanced magnetic resonance imaging (DCE-MRI) are widely used in the orofacial region. Furthermore, quantitative analyses have proven useful. However, a few reports have described the correlation between DWI-derived parameters and DCE-MRI-derived parameters, and the results have been controversial.

Purpose: To evaluate the correlation among parameters obtained by DWI and DCE-MRI and to compare them between benign and malignant lesions.

Material and Methods: Fifty orofacial lesions were analysed. The apparent diffusion coefficient (ADC), true diffusion coefficient (D), pseudodiffusion coefficient (D*) and perfusion fraction (f) were estimated by DWI. For DCE-MRI, TK model analysis was performed to estimate physiological parameters, for example, the influx forward volume transfer constant into the extracellular-extravascular space (EES) (K^{trans}) and fractional volumes of EES and plasma components (ve and vp).

Results: Both ADC and D showed a moderate positive correlation with ve ($\rho = 0.640$ and 0.645 , respectively). K^{trans} showed a marginally weak correlation with f ($\rho = 0.296$), while vp was not correlated with f or D*; therefore, IVIM perfusion-related parameters and TK model perfusion-related parameters were not straightforward. Both D and ve yielded high diagnostic power between benign lesions and malignant tumours with areas under the curve (AUCs) of 0.830 and 0.782, respectively.

¹Section of Oral and Maxillofacial Radiology, Division of Maxillofacial Diagnostic and Surgical Sciences, Faculty of Dental Science, Kyushu University, Fukuoka, Japan

²Department of Medical Technology, Kyushu University Hospital, Fukuoka, Japan

³Department of Molecular Imaging & Diagnosis, Graduate School of Medical Sciences, Kyushu University, Fukuoka, Japan

⁴Section of Oral and Maxillofacial Oncology, Division of Maxillofacial Diagnostic and Surgical Sciences, Faculty of Dental Science, Kyushu University, Fukuoka, Japan

⁵Laboratory of Oral Pathology, Division of Maxillofacial Diagnostic and Surgical Sciences, Faculty of Dental Science, Kyushu University, Fukuoka, Japan

Corresponding author:

Toru Chikui, Section of Oral and Maxillofacial Radiology, Faculty of Dental Science, Kyushu University, 3-1-1 Maidashi, Higashi-ku, Fukuoka 812-8582, Japan.

Email: chikui@rad.dent.kyushu-u.ac.jp



Creative Commons Non Commercial CC BY-NC: This article is distributed under the terms of the Creative Commons Attribution-NonCommercial 4.0 License (<https://creativecommons.org/licenses/by-nc/4.0/>) which permits non-commercial use, reproduction and distribution of the work without further permission provided the original work is attributed as specified on the SAGE and Open Access pages (<https://us.sagepub.com/en-us/nam/open-access-at-sage>).

Conclusion: Both D and ve were reliable parameters that were useful for the differential diagnosis. In addition, the true diffusion coefficient (D) was affected by the fractional volume of EES.

Keywords

Head and neck, tissue characterization, MR diffusion and perfusion

Received 4 October 2023; accepted 18 March 2024

Introduction

Diffusion-weighted imaging (DWI) and dynamic contrast-enhanced magnetic resonance imaging (DCE-MRI) are widely used throughout the human body, including in the head and neck region. Furthermore, quantitative analyses have proven useful for various purposes, such as differential diagnoses,^{1–3} metastatic lymph node evaluations and predicting the chemoradiotherapy response.^{4–6}

The apparent diffusion coefficient (ADC) has been widely used in clinical situations. Many reports have shown a negative correlation with the ADC and the absolute number of cells per square millimetre; in addition, a positive correlation has been reported with the percentage area of stroma.^{7–10} Intravoxel incoherent motion (IVIM) is attractive by virtue of its ability to elucidate both tissue diffusivity and perfusion, which yield the true diffusion coefficient (D), pseudodiffusion coefficient (D^*) and perfusion fraction (f).^{11–17}

In the quantitative analysis of DCE-MRI findings, the conventional assessment involves the estimation of parameters based on the time-intensity curve (TIC), such as the time of arrival of contrast agent (CA) (T_0), time to peak (TTP), maximum relative enhancement (MAXRELENH) and wash-in rate (WASHIN). However, this does not provide information on the underlying pharmacokinetic parameters in the tissue. Therefore, several different pharmacokinetic analyses have been proposed,¹⁸ with the Tofts and Kermode (TK) model proving to be one of the most popular, as it yields three physiological parameters: the influx forward volume transfer constant into the extracellular-extravascular space (EES) from the plasma (K^{trans}), the fractional volume of the EES per unit volume of tissue (ve) and the fractional volume of the plasma per unit volume of tissue (vp).^{19,20}

Given the above, we postulated that ve was correlated with both ADC and D . We further postulated that TK model perfusion-related parameters (K^{trans} and vp) were correlated with IVIM perfusion-related parameters. However, only a few reports have described the correlation between DWI-derived parameters and DCE-MRI-derived parameters, and the results have been controversial.^{21–26}

In addition, echoplanar (EPI)-DWI has been widely used. However, EPI-DWI causes signal loss and image

distortion due to magnetic inhomogeneity in the orofacial region. Alternative acquisition methods that are less strongly influenced by susceptibility artifacts, such as turbo spin-echo (TSE)-DWI, have been recommended.^{27,28} To our knowledge, no reports have evaluated the relationship between parameters obtained from TSE-DWIs and those obtained from DCE MRIs.

Thus, the present study evaluated the correlation between TSE-DWI-derived parameters and DCE-derived parameters and compared them between benign and malignant lesions.

Methods and materials

Study population

The ethics committee of our institution approved this retrospective study (no. 22025-02) and the need for informed consent was waived. The study plans were published on our institutional website. The patients had a right to decline to participate. The inclusion criteria were as follows: (a) all patients who consulted the Department of Oral and Maxillofacial Surgery from January 2021 to May 2023; (b) all patients with orofacial lesions who underwent MRI, including DCE-MRI and TSE-DWI; (c) patients whose lesion was visible on T1- and T2-weighted imaging; and (d) patients whose lesion had not been treated or recurred.

The exclusion criteria were as follows: (a) absence of a final diagnosis; (b) severe susceptibility artifacts; and (c) severe movement artifacts.

Imaging protocol

The MRI protocol was performed using a 3.0-Tesla MRI scanner (Achieva dStream, Ingenia and Ingenia Elition X; Philips Healthcare, Best, the Netherlands) with a 32-channel neurovascular coil.

DWI acquisition used a single-shot TSE protocol with 6 b-values of 0, 75, 150, 300, 500 and 1000 s/mm². Other parameters were as follows: repetition time (TR) = 3000–3575 ms; echo time (TE) = 77.6–87.4 ms, number of acquisitions = 2; TSE factor = 26; field of view = 230 × 230; slice thickness = 5 mm; slice gap = 1 mm, acquisition matrix = 128 × 105; matrix reconstruction = 224 × 224;

parallel imaging acceleration factor = 2; total scan duration = 300–367 s.

DCE-MRI used a three-dimensional T₁ fast-field echo sequence. The representative parameters were TR = 6.1 msec; TE = 2.3 msec; flip angle = 15°; field of view = 220 mm; slice thickness = 6 mm; slice number = 11; reduction factor of Compressed SENSE reduction factor = 4.5; acquisition voxel (mm) = 1.72 × 1.84 × 6.00; and reconstruction voxel (mm) = 0.86 × 0.86 × 6.00. Thirty seconds after the start of data acquisition, the operator initiated the injection of CA. We obtained 150 phases with a temporal resolution of 1.97 seconds. Gadobutrol (Gd-DO3A butrol) (Gadovist®; Bayer Healthcare, Berlin, Germany) was administered at a dose of 0.1 mmol/kg at a rate of 1 mL/s, immediately followed by a 20-mL saline flush. A reference precontrast scan was acquired prior to the DCE-MRI scan. The scan parameters were identical to those of the DCE scan, except for the flip angle, which was 5°. The

reference scan was also used to estimate the precontrast T₁ map using the image data with two different flip angles.

Estimation of DWI-derived parameters

All data obtained via TSE-DWI in the DICOM format were transferred to a personal computer for analyses. The ADC, D, D* and f were estimated. These procedures were performed using the OsiriX MD software program, version 12.5.0 (Pixmeo SARL, Bernex, Switzerland) (Figure 1).

Estimation of the DCE-derived parameters

A nonmodel analysis was first performed, directly analysing the change in the signal intensity during DCE-MRI. The representative parameters (T₀, TTP, MAXRELENH and WASHIN) were estimated using an MR T₁ perfusion

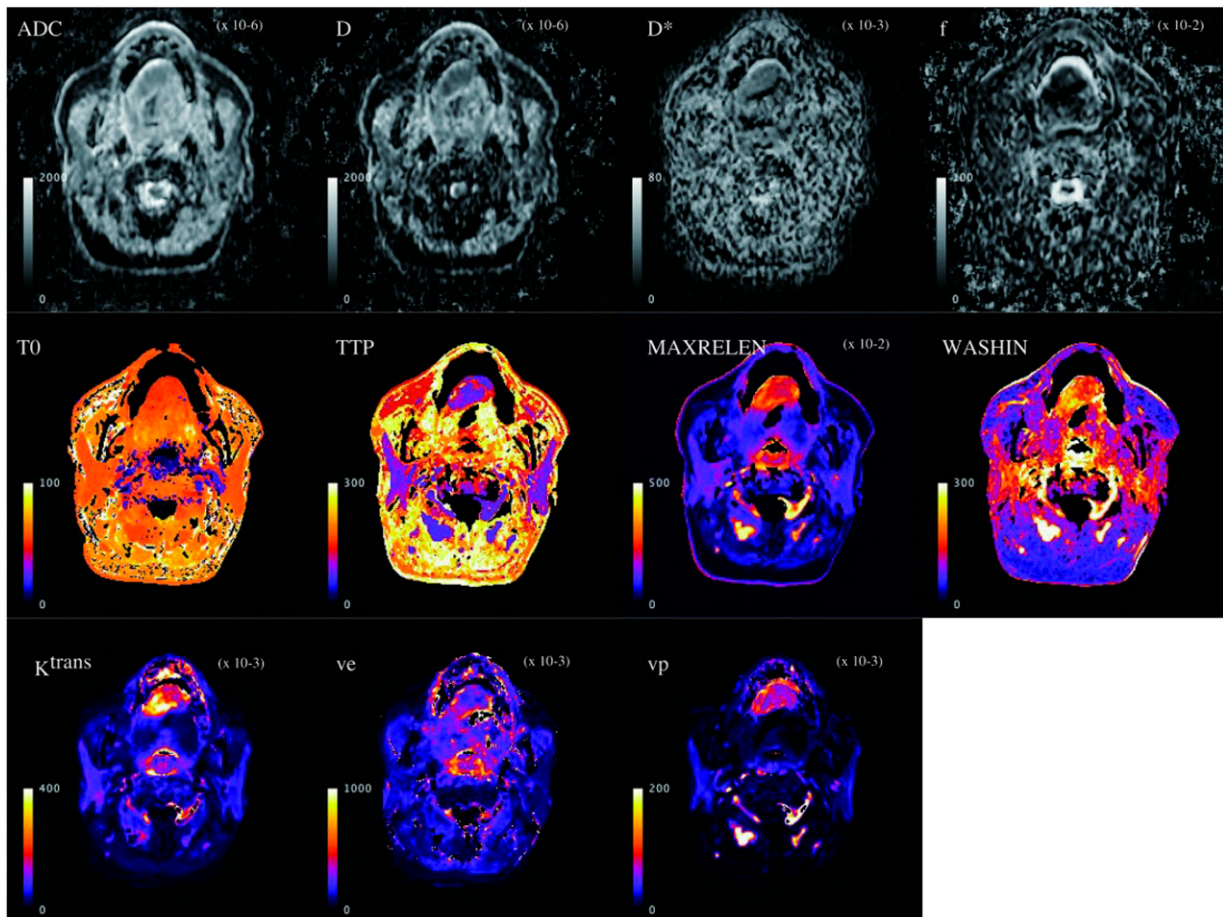


Figure 1. A 70-year-old woman with salivary duct carcinoma at the tongue. The ADC, D, D* and f were obtained by TSE-DWI. This lesion had ADC, D, D*, and f values of $1.06 \times 10^{-3} \text{ mm}^2/\text{s}$, $0.772 \times 10^{-3} \text{ mm}^2/\text{s}$, $32.5 \times 10^{-3} \text{ mm}^2/\text{s}$ and 0.31, respectively. The T₀, TTP, MAXRELENH and WASHIN were obtained by a T₁ perfusion analysis. This lesion had T₀, TTP, MAXRELENH, and WASHIN values of 51.1 s, 86.4 s, 2.35 and 180, respectively. The K^{trans} , ve and vp were obtained by a TK model analysis. K^{trans} was 0.226 min^{-1} , ve was 0.252 and vp was 0.068. High perfusion-related parameters (f, K^{trans} and vp) and low D values were characteristic of this lesion.

software program in the workstation (Intelli Space Portal version 6; Philips Healthcare). (Figure 1).

A pharmacokinetic analysis based on the TK model was then performed to estimate the three parameters of K^{trans} , v_e and v_p .^{19,20} These procedures were processed using a software program in the PAR/REC format (PRIDE software; Philips Healthcare). We set the r_1 relaxivity of Gadovist to 5.0 mM/sec. (Figure 1).

Region of interest setting

All parameter maps were transferred to a personal computer for the ROI settings. Both the FOVs and matrix size of the DWI-derived parameter maps were matched to those of the DCE-MRI-derived parameter maps. An observer who was blinded to the final diagnosis selected the slice with the maximum area and manually drew a freehand ROI to circumvent the lesions. An observer with 28 years of experience in head and neck radiology set the ROI twice with an interval of at least 1 month.

For DWI scans, the ROI was placed with $b = 0$ s/mm² by referencing the T2-weighted images, avoiding large vessels and necrotic areas. The ROIs were copied to all DWI-derived parameter maps. For the DCE-derived parameters, the ROI was placed on a dynamic image that clearly showed the contour of the lesion. The ROIs were then copied to all DCE-derived parameter maps. The ImageJ software program, version 1.5, was used for the ROI setting and measurement of the parameters.

Statistical analyses

The observers recorded the median of all estimated parameters. The intraobserver reliability was assessed by the intraclass correlation coefficient (ICC) with the 95% confidence interval (CI). The quantitative values obtained from two measurements were then averaged for further analyses. The correlation between the parameters was evaluated by Spearman's rank correlation coefficient. The interpretations of the correlation coefficient (ρ) were as follows: 0.00–0.20, negligible correlation; 0.20–0.40, weak correlation; 0.40–0.70, moderate correlation; and 0.70–1.00, strong correlation. The quantitative values of all parameters were compared between two categories by Wilcoxon's signed-rank sum test. We also performed a receiver operative curve (ROC) analysis to evaluate the diagnostic performance of three different quantifications (DWI-derived parameter, T1 perfusion-derived parameters and TK model-derived parameters) in differentiating benign from malignant lesions.

We performed all statistical analyses using the JMP Pro software program, version 16.0.0 (SAS Institute, Cary, NC, USA) and the SPSS Statistics software program, version 27.0 (IBM Corporation, Armonk, NY, USA). P values of <0.05 were accepted as statistically significant.

Results

Fifty patients were analysed in this study (male, $n = 29$; female, $n = 21$; average age, 59.8 ± 18.3 years old). Of the 50 total lesions, 32 were malignant tumours (squamous cell carcinoma [SCC], $n = 25$; malignant salivary gland tumours [MSGT] $n = 5$; adenocarcinoma, $n = 1$; malignant lymphoma [ML] $n = 1$). Eighteen lesions were benign (pleomorphic adenoma, $n = 6$; schwannoma, $n = 3$; ameloblastoma, $n = 2$; angioleiomyoma $n = 1$; vascular abnormality [VA], $n = 1$ and granulation tissue, $n = 5$). The final diagnosis was obtained from either a surgical specimen ($n = 39$), incisional biopsy ($n = 10$) or image diagnosis and clinical follow-up (VA, $n = 1$). The lesions were in the tongue ($n = 12$), buccal space ($n = 11$), maxilla ($n = 9$), mandible ($n = 6$), oral floor ($n = 5$), lip ($n = 2$), parotid space ($n = 1$), submandibular space ($n = 1$), oropharynx ($n = 1$) and upper neck ($n = 2$). The sizes of the ROI on DWI and DCE-11 were 301 ± 209 mm² and 278 ± 190 mm², respectively.

The ICCs were excellent for both DWI-derived parameters (ADC = 0.984, D = 0.991, D* = 0.947 and f = 0.968) and T1 perfusion-derived parameters (T0 = 0.990, TTP = .987, MAXRELENH = 0.988 and WASHIN = 0.994). The ICCs for the TK model-derived parameters were also excellent ($K^{\text{trans}} = 0.977$, $v_p = .997$, and $v_e = .993$). Therefore, the average values obtained from the two measurements were used in further statistical analyses.

Correlations among DCE-MRI-derived parameters (T1 perfusion analysis vs. TK model analysis)

All parameters' correlation coefficients are shown in Table 1. T0 showed a marginally significant weak negative correlation with v_p ($\rho = -0.286$, $p = .044$); however, correlations between T0 and TK model-derived parameters were poor. TTP had a moderate negative correlation with K^{trans} and v_p ($\rho = -0.428$ and -0.664 , respectively) and a moderate positive correlation with v_e ($\rho = 0.582$). MAXRELENH showed a significant moderate to strong positive correlation with K^{trans} , v_e and v_p ($\rho = 0.799$, 0.588 and 0.422, respectively), which seems reasonable. WASHIN showed a significant weak to moderate positive correlation with K^{trans} and v_p ($\rho = 0.383$ and 0.666, respectively) and a weak negative correlation with v_e ($\rho = -0.337$), and this trend was opposite to that of TTP.

Correlations between T1 perfusion-derived parameters and DWI-derived parameters

MAXRELENH showed a weak positive correlation with IVIM perfusion-related parameters (D*; $\rho = 0.363$ and f; 0.315, respectively). MAXRELENH also showed a weak to moderate positive correlation with ADC and D ($\rho = 0.416$ and 0.340, respectively). However, no other

Table 1. Correlations between T1 perfusion-derived parameters and TK model-derived parameters.

	T0		TTP		MAXRELENH		WASHIN	
	ρ	p	ρ	p	ρ	p	ρ	p
K^{trans}	-0.229	0.110	-0.428*	0.002	0.799*	<.0001	0.383*	0.0061
Ve	0.070	0.6284	0.582*	<.0001	0.588*	<.0001	-0.337*	0.0166
Vp	-0.286*	0.044	-0.664*	<.0001	0.422*	0.0023	0.666*	<.0001

ρ , Spearman's rank-order correlations; T0, time of arrival; TTP, time to peak; MAXRELENH, maximum relative enhancement; WASHIN, wash-in rate; K^{trans} , the influx forward volume transfer constant into the EES from the plasma; ve, the fractional volume of EES; vp, the fractional volume of plasma. *statistically significant difference ($p < .05$).

Table 2. Correlations between T1 perfusion-derived parameters and DWI-derived parameters.

	T0		TTP		MAXRELENH		WASHIN	
	ρ	p	ρ	p	ρ	p	ρ	p
ADC	-0.092	0.524	0.269	0.059	0.416*	0.003	-0.203	0.158
D	-0.049	0.733	0.312*	0.027	0.340*	0.016	-0.254	0.075
D*	-0.019	0.898	0.182	0.206	0.363*	0.010	-0.110	0.445
f	-0.047	0.749	-0.095	0.514	0.315*	0.026	0.086	0.555

ρ , Spearman's rank-order correlations; T0, time of arrival; TTP, time to peak; MAXRELENH, maximum relative enhancement; WASHIN, wash-in rate; ADC, apparent diffusion coefficient; D, true diffusion coefficient; D*, pseudo diffusion coefficient; f, perfusion fraction. *statistically significant difference ($p < .05$).

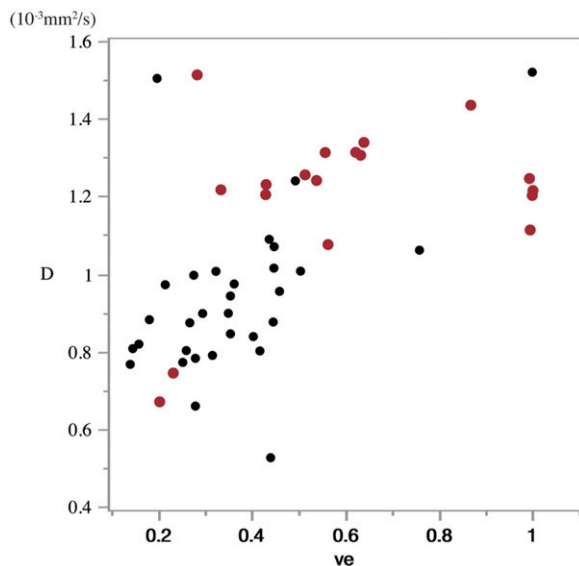


Figure 2. Two-dimensional plot of the true diffusion coefficient (D) and fractional volume of the extravascular-extracellular component (ve). D had a moderate positive correlation with ve ($\rho = 0.645$). The black mark shows a malignant lesion, and the red mark shows a benign lesion.

T1 perfusion-derived parameters showed any significant correlation with DWI-derived parameters except for the weak correlation between TTP and D. The details of the coefficient values are shown in Table 2.

Correlations between TK model-derived parameters and DWI-derived parameters

Both the ADC and D showed a moderate positive correlation with ve ($\rho = 0.640$ and 0.645 , respectively) (Figure 2). These results demonstrated that the increase in the EES resulted in an increase in ADC and D. Concerning the perfusion-related parameters, K^{trans} showed a weak positive correlation with f ($\rho = 0.296$, $p = .037$). The details are shown in Table 3.

Comparisons of the parameters between benign and malignant lesions

Table 4 shows the comparison of the parameters between benign and malignant entities. Benign lesions had a significantly higher ADC, D, TTP and ve than malignant lesions ($p = .0001$, $.0001$, 0.0009 and 0.0009 , respectively). Conversely, benign lesions had a significantly lower WASHIN and vp than malignant lesions ($p = .0279$ and $.016$, respectively). Due to high f and K^{trans} in VA, angioleiomyoma, and granulation tissue, significant differences were not found between benign and malignant lesions in either f or K^{trans} (Supplementary table 1).

A multiple regression analysis using a stepwise procedure selected D from among DWI-derived parameters, TTP from among T1 perfusion-derived parameters and ve from among TK model-derived parameters. The area under the

curve (AUC) is shown in Table 5. No significant difference was found among the three quantitative methods (DWI vs. T1 perfusion, $p = .580$; DWI vs. TK model, $p = .426$; and T1 perfusion vs. TK model, $p = .991$). When including all parameters, both D and TTP were selected as predictive parameters (AUC = 0.854); however, the diagnostic power

was not improved (DWI vs. all, $p = .471$; TK model vs. all, $p = .142$; and T1 perfusion vs. all, $p = .267$).

Discussion

The present study evaluated the correlations between DWI- and DCE-MRI-derived parameters. First, we evaluated the correlation between T1 perfusion-derived parameters and TK model-derived parameters (Table 1). Immediately after the arrival of the CA, the CA predominantly exists in the intravascular space; however, it leaks into the EES as time passes. Therefore, the negative correlation of the TTP with both K^{trans} and vp and its positive correlation with ve is considered reasonable. MAXRELENH showed not only a positive correlation with perfusion-related TK model parameters (K^{trans} and vp) but also a correlation with ve. WASHIN showed a significant positive correlation with both K^{trans} and vp but a weak negative correlation with ve, and this trend was opposite to that of TTP.

T1 perfusion-derived parameters, except MAXRELENH, were less related to DWI-derived parameters. It was thus very difficult to link the DWI-derived parameters to T1 perfusion-derived parameters that did not directly reflect

Table 3. Correlations between TK model-derived parameters and DWI-derived parameters.

	K^{trans}		ve		vp	
	ρ	p	ρ	p	ρ	p
ADC	0.202	0.159	0.640*	<.0001	-0.135	0.351
D	0.140	0.332	0.645*	<.0001	-0.185	0.200
D*	0.218	0.129	0.409*	0.003	-0.074	0.611
f	0.296*	0.037	0.100	0.491	0.144	0.320

ρ , Spearman's rank-order correlations; K^{trans} , the influx forward volume transfer constant into the EES from the plasma; ve, the fractional volume of EES; vp, the fractional volume of plasma; ADC, apparent diffusion coefficient; D, true diffusion coefficient; D*, pseudo diffusion coefficient; f, perfusion fraction.

*statistically significant difference ($p < .05$).

Table 4. A comparison of the parameters between benign and malignant entities.

	Benign	Malignant	p value
Diffusion-derived parameters			
ADC ($\times 10^{-3}$ mm ² /s)	1.34 \pm 0.23	1.07 \pm 0.20	0.0001*
D ($\times 10^{-3}$ mm ² /s)	1.20 \pm 0.20	0.93 \pm 0.21	0.0001*
D* ($\times 10^{-3}$ mm ² /s)	40.08 \pm 5.90	37.66 \pm 7.53	0.412
f	0.16 \pm 0.09	0.16 \pm 0.06	0.610
T1 perfusion-derived parameters			
T0 (s)	49.96 \pm 9.9	51.5 \pm 4.3	0.9441
TTP (s)	217.1 \pm 61.2	152.6 \pm 61.6	0.0009*
MAXRELENH	2.17 \pm 0.58	2.11 \pm 0.51	0.842
WASHIN	99.9 \pm 57.1	130.4 \pm 63.0	0.0279*
TK model-derived parameters			
K^{trans} (min ⁻¹)	0.159 \pm 0.115	0.162 \pm 0.064	0.187
ve	0.595 \pm 0.264	0.363 \pm 0.176	0.0009*
vp	0.030 \pm 0.018	0.050 \pm 0.032	0.016*

ADC, apparent diffusion coefficient; D, true diffusion coefficient; D*, pseudo diffusion coefficient; f, perfusion fraction; T0, time of arrival; TTP, time to peak; MAXRELENH, maximum relative enhancement; WASHIN, wash-in rate; K^{trans} , the influx forward volume transfer constant into the EES from the plasma; ve, the fractional volume of EES; vp, the fractional volume of plasma.

Table 5. Diagnostic performance (AUC) in discriminating benign lesions from malignant lesions.

	Selected parameters	mean	Standard error	Lower limit of 95% CI	Upper limit of 95% CI
DWI-derived parameters	D	0.830	0.075	0.634	0.932
T1 perfusion-derived parameters	TTP	0.783	0.067	0.625	0.886
TK model-derived parameters	ve	0.782	0.073	0.608	0.893
All parameters	D + TTP	0.854	0.067	0.671	0.944

AUC, area under the curve; ADC, apparent diffusion coefficient; TTP, time to peak; ve, the fractional volume of EES; CI, confidence interval.

the underlying physiological condition. These results were in line with those of previous reports.^{21,22} In contrast, the pharmacokinetic analysis revealed several correlations with DWI-derived parameters. An increase in v_e increased the ADC. White demonstrated that the ADC values were inversely correlated with tumour cellularity, showing a Pearson's correlation coefficient of 0.556. Their study included 24 lesions of the nasal cavity and the paranasal sinuses.⁹ Driessen et al. separated digitized haematoxylin-eosin-stained sections of laryngeal and hypopharyngeal carcinoma into nuclei, cytoplasm and stroma using colour-based segmentation. The percentage of stroma area was correlated with the ADC, while the percentage of nuclei area was inversely correlated with the ADC (Spearman's correlation coefficient = 0.69 and -0.64, respectively).⁸ These results were in line with our own findings (Table 3).

In the present study, D also had a significant moderate positive correlation with v_e . This result is compatible with the previous report by Li et al., who demonstrated the close negative correlation between the D value and the tumour-to stroma ratio in patients with early cervical carcinoma.²⁹

Several studies have shown that IVIM perfusion-related parameters correlate with perfusion-related parameters obtained by dynamic susceptibility contrast MRI for the evaluation of cerebral perfusion,^{30,31} where the leakage of CA into the EES can be considered negligible. However, such leakage cannot be discounted for the evaluation of tumorous lesions. Our research showed that K^{trans} had a significant weak positive correlation with f . Most previous research has also failed to demonstrate any strong, straightforward correlation.^{21-24,32}

In a physiological sense, K^{trans} reflects the tissue blood flow if tissue perfusion is low relative to the permeability surface area product (PSAP) and conversely will reflect permeability if tissue perfusion is high relative to the PSAP,^{19,32} therefore, we considered that a weak correlation seems to be reasonable.

Unexpectedly, we noted no significant positive correlation between v_p and IVIM perfusion-related parameters. However, this is consistent with the findings of previous reports.^{24,25,32} The signal intensity from all vessels was included in the DCE-MRI analysis, whereas the IVIM analysis assumed that the perfusion-related parameters were estimated from the signal intensity of the capillaries.¹³⁻¹⁵ Such conceptual differences might have resulted in the lack of a significant correlation between these parameters.

Both ADC and D were also useful for differentiating benign and malignant lesions, and they were correlated with v_e . These findings were in line with much previous research. In general, many studies have reported that the K^{trans} and f values of malignant lesions are larger than those of benign lesions; however, there was no significant difference between them, which is probably due to the wide variation in

benign lesions. In the present study, we found no improvement in diagnostic ability by combining DWI and DCE-MRI. However, if we focus on diseases of specific organs such as the parotid gland, thyroid gland,³³ paranasal sinus^{34,35} and so on, we believe that there might be a possibility of improving diagnostic performance by combining them.

Several limitations associated with the present study warrant mention. First, the ROIs of the DWI-derived parameter map were not identical to those of the DCE-MRI-derived map. The slice thickness of 3-dimensional DCE-MRI was 6 mm, whereas that of multislice TSE-DWI was 5 mm with a 1-mm slice gap. This issue might have reduced the correlation between the parameters obtained by the two sequences. Second, cases with severe movement were excluded from the study population; however, the unrecognized artifacts might have influenced the parameters. Third, the lack of standardization for the quantification might have affected the quantification. The TK model used in the DCE-MRI analysis was technically challenging and carried a risk of being confounded by many factors. Fourth, we used TSE-DWI with six b values due to the extended acquisition time; however, the selection of the b values influences the IVIM parameters. In addition, the long acquisition time and complex signal acquisition method associated with TSE-DWI might have influenced the DWI perfusion-related parameters.^{27,28} However, the optimization of TSE-DWI is beyond the scope of this preliminary study.

In conclusion, both D and v_e were reliable parameters that were useful for the differential diagnosis; in addition, there was a significant positive correlation between them. Conversely, IVIM perfusion-related parameters and TK model perfusion-related parameters were not straightforward.

Acknowledgements

We used a software program (PRIDE software, Philips) using the interface data language (IDL, RSL).

Declaration of conflicting interests

The author(s) declared the following potential conflicts of interest with respect to the research, authorship, and/or publication of this article: We used a software program (PRIDE software, Philips) using the interface data language (IDL, RSL), which was proprietary software program and has been developed as collaborative research between Philips and Kyushu University. At present, the software program for commercial use has been marketed. Therefore, we were allowed to use PRIDE software without any contrast with Philips. We have got the agreement on it from Philips Healthcare.

Funding

The author(s) disclosed receipt of the following financial support for the research, authorship, and/or publication of this article: This study was supported by a Ministry of Education, Culture, Sports, Science and Technology Grant-in-Aid for Scientific Research (C) 18K09770.

Declaration of generative AI in scientific writing

We declare that we did not use any generative AI or AI-assisted technologies in the writing process.

ORCID iDs

Toru Chikui  <https://orcid.org/0000-0002-3457-7719>

Yukiko Kami  <https://orcid.org/0000-0003-0092-7239>

Supplemental Material

Supplemental material for this article is available online.

References

1. Yabuuchi H, Fukuya T, Tajima T, et al. Salivary gland tumors: diagnostic value of gadolinium-enhanced dynamic MR imaging with histopathologic correlation. *Radiology* 2003; 226: 345–354.
2. Yabuuchi H, Kamitani T, Sagiya K, et al. Characterization of parotid gland tumors: added value of permeability MR imaging to DWI and DCE-MRI. *Eur Radiol* 2020; 30: 6402–6412.
3. Kitamoto E, Chikui T, Kawano S, et al. The application of dynamic contrast-enhanced MRI and diffusion-weighted MRI in patients with maxillofacial tumors. *Acad Radiol*. 2015; 22: 210–216.
4. King AD, Mo FK, Yu KH, et al. Squamous cell carcinoma of the head and neck: diffusion-weighted MR imaging for prediction and monitoring of treatment response. *Eur Radiol* 2010; 20: 2213–2220.
5. Kim S, Loevner L, Quon H, et al. Diffusion-weighted magnetic resonance imaging for predicting and detecting early response to chemoradiation therapy of squamous cell carcinomas of the head and neck. *Clin Cancer Res* 2009; 15: 986–994.
6. Chikui T, Kitamoto E, Kawano S, et al. Pharmacokinetic analysis based on dynamic contrast-enhanced MRI for evaluating tumor response to preoperative therapy for oral cancer. *J Magn Reson Imaging*. 2012; 36: 589–597.
7. Surov A, Meyer HJ, Wienke A. Correlation between apparent diffusion coefficient (ADC) and cellularity is different in several tumors: a meta-analysis. *Oncotarget* 2017; 8: 59492–59499.
8. Driessen JP, Caldas-Magalhaes J, Janssen LM, et al. Diffusion-weighted MR imaging in laryngeal and hypopharyngeal carcinoma: association between apparent diffusion coefficient and histologic findings. *Radiology* 2014; 272: 456–463.
9. White ML, Zhang Y, Robinson RA. Evaluating tumors and tumorlike lesions of the nasal cavity, the paranasal sinuses, and the adjacent skull base with diffusion-weighted MRI. *J Comput Assist Tomogr* 2006; 30: 490–495.
10. Surov A, Meyer HJ, Winter K, et al. Histogram analysis parameters of apparent diffusion coefficient reflect tumor cellularity and proliferation activity in head and neck squamous cell carcinoma. *Oncotarget* 2018; 9: 23599–23607.
11. Yuan J, Yeung DKW, Mok GS, et al. Non-Gaussian analysis of diffusion weighted imaging in head and neck at 3T: a pilot study in patients with nasopharyngeal carcinoma. *PLoS One* 2014; 9: e87024.
12. Jansen JF, Stambuk HE, Koutcher JA, et al. Non-Gaussian analysis of diffusion-weighted MR imaging in head and neck squamous cell carcinoma: a feasibility study. *AJNR Am J Neuroradiol* 2010; 31: 741–748.
13. Le Bihan D, Breton E, Lallemand D, et al. MR imaging of intravoxel incoherent motions: application to diffusion and perfusion in neurologic disorders. *Radiology* 1986; 161: 401–407.
14. Le Bihan D, Breton E, Lallemand D, et al. Separation of diffusion and perfusion in intravoxel incoherent motion MR imaging. *Radiology* 1988; 168: 497–505.
15. Le Bihan D, Turner R. The capillary network: a link between IVIM and classical perfusion. *Magn Reson Med* 1992; 27: 171–178.
16. Liang L, Luo X, Lian Z, et al. Lymph node metastasis in head and neck squamous carcinoma: efficacy of intravoxel incoherent motion magnetic resonance imaging for the differential diagnosis. *Eur J Radiol* 2017; 90: 159–165.
17. Sumi M, Nakamura T. Head and neck tumors: assessment of perfusion-related parameters and diffusion coefficients based on the intravoxel incoherent motion model. *Am J Neuroradiol* 2013; 34: 410–416.
18. Sourbron SP, Buckley DL. Tracer kinetic modelling in MRI: estimating perfusion and capillary permeability. *Phys Med Biol* 2012; 57: R1–33.
19. Tofts PS, Brix G, Buckley DL, et al. Estimating kinetic parameters from dynamic contrast-enhanced T₁-weighted MRI of a diffusable tracer: standardized quantities and symbols. *J Magn Reson Imag* 1999; 10: 223–232.
20. Tofts PS. Modelling tracer kinetics in dynamic Gd-DTPA MR imaging. *J Magn Reson Imag* 1997; 7: 91–101.
21. Xu XQ, Choi YJ, Sung YS, et al. Intravoxel incoherent motion MR imaging in the head and neck: correlation with dynamic contrast-enhanced MR imaging and diffusion-weighted imaging. *Korean J Radiol* 2016; 17: 641–649.
22. Marzi S, Piludu F, Forina C, et al. Correlation study between intravoxel incoherent motion MRI and dynamic contrast-enhanced MRI in head and neck squamous cell carcinoma: evaluation in primary tumors and metastatic nodes. *Magn Reson Imaging* 2017; 37: 1–8.

23. Fujima N, Sakashita T, Homma A, et al. Advanced diffusion models in head and neck squamous cell carcinoma patients: goodness of fit, relationships among diffusion parameters and comparison with dynamic contrast-enhanced perfusion. *Magn Reson Imaging* 2017; 36: 16–23.
24. Zhong Y, Xiao Z, Tang Z, et al. Intravoxel incoherent motion MRI for differentiating sinonasal small round cell malignant tumours (SRCMTs) from Non-SRCMTs: comparison and correlation with dynamic contrast-enhanced MRI. *Clin Radiol* 2018; 73: 966–974.
25. Sun H, Xu Y, Xu Q, et al. Correlation between intravoxel incoherent motion and dynamic contrast-enhanced magnetic resonance imaging parameters in rectal cancer. *Acad Radiol* 2019; 26: e134–e140.
26. Marzi S, Stefanetti L, Sperati F, et al. Relationship between diffusion parameters derived from intravoxel incoherent motion MRI and perfusion measured by dynamic contrast-enhanced MRI of soft tissue tumors. *NMR Biomed* 2016; 29: 6–14.
27. Panyarak W, Chikui T, Yamashita Y, et al. Image Quality and ADC Assessment in Turbo Spin-Echo and Echo-Planar Diffusion-Weighted MR Imaging of Tumors of the Head and Neck. *Acad Radiol*. 2019; 26: e305–e316.
28. Mikayama R, Yabuuchi H, Sonoda S, et al. Comparison of intravoxel incoherent motion diffusion-weighted imaging between turbo spin-echo and echo-planar imaging of the head and neck. *Eur Radiol* 2018; 28: 316–324.
29. Li X, Wang P, Li D, et al. Intravoxel incoherent motion MR imaging of early cervical carcinoma: correlation between imaging parameters and tumor-stroma ratio. *Eur Radiol* 2018; 28: 1875–1883.
30. Wu WC, Chen YF, Tseng HM, et al. Caveat of measuring perfusion indexes using intravoxel incoherent motion magnetic resonance imaging in the human brain. *Eur Radiol* 2015; 25: 2485–2492.
31. Federau C, O'Brien K, Meuli R, et al. Measuring brain perfusion with intravoxel incoherent motion (IVIM): initial clinical experience. *J Magn Reson Imag* 2014; 39: 624–632.
32. Bakke KM, Grøvik E, Meltzer S, et al. Comparison of Intravoxel incoherent motion imaging and multiecho dynamic contrast-based MRI in rectal cancer. *J Magn Reson Imag* 2019; 50: 1114–1124.
33. Song M, Yue Y, Guo J, et al. Quantitative analyses of the correlation between dynamic contrast-enhanced MRI and intravoxel incoherent motion DWI in thyroid nodules. *Am J Transl Res* 2020; 15: 3984–3992.
34. Wang F, Sha Y, Zhao M, et al. High-resolution diffusion-weighted imaging improves the diagnostic accuracy of dynamic contrast-enhanced sinonasal magnetic resonance imaging. *J Comput Assist Tomogr* 2017; 41: 199–205.
35. Jiang J, Xiao Z, Tang Z, et al. Differentiating between benign and malignant sinonasal lesions using dynamic contrast-enhanced MRI and intravoxel incoherent motion. *Eur J Radiol* 2018; 98: 7–13.